

# Magneto-optical response of CdSe nanostructures

Po-Chung Chen and K. Birgitta W. Haley

Department of Chemistry and Pitzer Center for Theoretical Chemistry, University of California Berkeley  
(Dated: March 22, 2024)

We present theoretical calculations of the Lande  $g$ -factors of semiconductor nanostructures using a time-dependent empirical tight-binding method. The eigenenergies and eigenfunctions of the band edge states are calculated as a function of an external magnetic field with the electromagnetic field incorporated into the tight-binding Hamiltonian in a gauge-invariant form. The spin-orbit interaction and magnetic field are treated non-perturbatively. The  $g$ -factors are extracted from the energy splitting of the eigenstates induced by the applied magnetic field. Both electron and hole  $g$ -factors are investigated for CdSe nanostructures. The size and aspect ratio dependence of  $g$ -factors is studied. We observe that the electron  $g$ -factors are anisotropic and find that the calculated values agree quantitatively with experimental data. We conclude that the two distinct  $g$ -factor values extracted from time-resolved Faraday rotation experiments should be assigned to the anisotropic in-plane ( $g_k$ ) and out-of-plane ( $g_z$ ) electron  $g$ -factors, rather than to isotropic electron and exciton  $g$ -factors. We find that the anisotropy in the electron  $g$ -factor depends on the aspect ratio of the nanocrystal. The  $g$ -factor anisotropy derived from the wurtzite structure and from the non-unity aspect ratio may cancel each other in some regime. We observe that hole  $g$ -factors oscillate as a function of size, due to size-dependent mixing between the heavy hole-light hole components of the valence band edge states. Extension to the calculation of exciton  $g$ -factors is discussed.

## I. INTRODUCTION

Spin dynamics in semiconductor nanostructures have been studied intensively in recent years, motivated by the emerging field of semiconductor spintronics and quantum information processing.<sup>1</sup> The most important time scale when implementing the quantum computer is the decoherence time of the quantum degree of freedom which is intended to be used as the qubit. Typically the spin decoherence time in the bulk semiconductor material is extremely short. However, it is expected that the spin decoherence time should increase substantially in nanostructures due to the three-dimensional quantum confinement. This expectation is supported by the optical orientation experiments of Gupta et al.<sup>2</sup> where a nano-second spin lifetime was measured for neutral CdSe nanostructures. This indicates that there will be plenty of time to perform quantum operations on the spin degree of freedom in semiconductor nanostructure before the coherence is lost. Consequently spins in nanostructures are excellent candidates for qubits. On the other hand, both spin-based quantum computation and spintronics require precise control of the spin. Since the control of the spin dynamics in nanostructures is strongly dependent on the  $g$ -factors of electrons, holes, and excitons in the nanostructure, it is imperative to understand the behavior and magnitude of  $g$ -factors.

Experimentally the  $g$ -factors of CdSe nanocrystals with wurtzite lattice structure have been measured via Time-Resolved Faraday Rotation (TRFR)<sup>2,3</sup> and Magnetic Circular Dichroism (MCD).<sup>5</sup> The TRFR experiment measurement reveals multiple  $g$ -factors. Two or four distinct  $g$ -factor values are extracted, depending on the size of the nanostructure which ranges from 22 Å to 80 Å in diameter. The size distribution of the sample is about 5-15%.<sup>3,4</sup> The sample from 22 Å to 57 Å has a

size-dependent mean aspect ratio ranging from 1.0 to 1.3, with a 0.2 variation<sup>3,4,14</sup>. It was suggested that when there are four distinct  $g$ -factors, these  $g$ -factors should be assigned to anisotropic electron and exciton  $g$ -factors.<sup>2</sup> It has been speculated that there exists a quasispherical regime in which the  $g$ -factors become isotropic, hence reducing the number of distinct  $g$ -factors from four to two. On the other hand, MCD measurements reveal only a single exciton  $g$ -factor for nanocrystals with 19 Å and 25 Å in diameter.<sup>5</sup> It should be noted that the hole spin is also initially aligned by the optical pumping in a TRFR experiment. It has been argued that the fast decoherence of the hole spin makes it impossible to detect the hole  $g$ -factor in TRFR.<sup>2</sup> Although it is well established experimentally<sup>6</sup> and theoretically<sup>7</sup> that the hole spin decoherence time in the bulk semiconductor is extremely small, the three-dimensional quantum confinement might also alter significantly the hole spin decoherence time in the nanostructure. To the best of our knowledge there is neither experimental measurement nor theoretical estimation about the hole decoherence time in those nanostructures. Recent time-resolved photoluminescence on InAs/GaAs quantum dots<sup>8</sup> suggests that neither the electron nor the hole spin relax on the lifetime scale of the exciton in the system but no estimation of the hole relaxation time could be made. This suggests that a hole decoherence time becomes much longer in nanostructures. It is thus not yet clear whether the hole  $g$ -factor signature should appear in a TRFR experiment.

Theoretically, the size dependence of the electron  $g$ -factor in CdSe nanostructures has been calculated with the eight-band Kane model<sup>10,11,12</sup>, and in the tight-binding model.<sup>13,14</sup> In general, the effective mass approximation (EMA) type calculation is inadequate for nanostructures at small sizes ( $\leq 30$  Å) because the atomic nature and surface effects become more prominent as the

size of the nanostructure decreases. Because of its atomic nature, the tight-binding model is ideal to study the electronic and optical properties of nanostructures in this size range.

The time-independent tight-binding approach to calculation of  $g$ -factors in Ref 14 is based on Stone's formula<sup>15</sup> which is derived from the double second order perturbation in terms of the spin-orbit interaction and the external magnetic field. The results obtained from this perturbative analysis show strong shape dependence. It was observed that a transition from anisotropic to isotropic  $g$ -factor tensor occurs at aspect ratio 0.3, resulting in a quasispherical regime, as originally suggested by Rodina and coworkers.<sup>12</sup> Since the spin-orbit interaction is strong in CdSe, ( $C_d = 0.151\text{eV}$  and  $S_e = 0.320\text{eV}$ ), it is desirable to include this non-perturbatively in order to get quantitative values. This not only provides a more accurate estimation of the electron  $g$ -factors for nanostructures with strong spin-orbit interaction, but will also enable us to treat the hole and exciton  $g$ -factors systematically, in addition to the electron  $g$ -factors. It is also intriguing to investigate the possibility of a quasispherical regime in more quantitative calculations for the electron  $g$ -factor.

In this paper we present such non-perturbative theoretical calculations of the electron and hole  $g$ -factors for CdSe nanostructures employing the time-dependent empirical tight-binding theory. Both the spin-orbit interaction and the external magnetic field are taken into account non-perturbatively. The  $g$ -factors are extracted from the magnetic field induced energy shifts of the electron and hole eigenvalues. The size and aspect ratio dependence of the resulting  $g$ -factors is investigated. We observe that the electron  $g$ -factors decrease monotonically as a function of size and are strongly anisotropic. The calculated values agree well with the experimental data from TRFR. It will be shown that the electron  $g$ -factors can explain the TRFR experimental data without invoking a exciton  $g$ -factor. The result also shows partial cancellation between the anisotropy deriving from the wurtzite structure and from the aspect ratio. The hole  $g$ -factors show very different behavior. They show marked oscillations as a function of the size. This is due to the size sensitive mixing between the heavy hole and light hole components. The exciton  $g$ -factor is not included in the current calculation. However the same calculation scheme can be easily extended to calculate the exciton  $g$ -factor with Coulomb interactions included non-perturbatively.<sup>18,20</sup>

The paper is organized as follows: In section II we summarize the empirical tight-binding Hamiltonian for CdSe nanostructures and describe how to solve the model using a time-dependent approach. In section III we present our numerical results, including total density of states, band gap, and electron and hole  $g$ -factors. In section IV we draw several conclusions and discuss possible future directions.

## II. THEORY AND MODEL

### A. Tight-binding model of CdSe nanostructure

We start from the empirical tight-binding model for the bulk CdSe semiconductor with an  $sp_3s$  basis. The parameters we use for CdSe are derived from the empirical parameters obtained by Lippens and Lannoo<sup>17</sup> for the bulk CdSe in the zinc-blende structure, assuming nearest-neighbor interactions only. We construct the CdSe nanocrystals with wurtzite structure corresponding to the typical CdSe nanostructures seen in TEM images.<sup>16</sup> The constructed structures have approximate but not exact  $C_{3v}$  symmetry. The same structures have been used in previous time-independent tight-binding studies.<sup>14,19,21</sup> We remove the dangling bonds on the surface by shifting the energies of the corresponding hybrid orbitals well above the conduction band edge. The spin-orbit interaction is included in the Hamiltonian. Spin-orbit coupling constants are assigned to both types of atoms, with  $C_d = 0.151\text{eV}$  and  $S_e = 0.320\text{eV}$  respectively.<sup>21,25</sup> In order to reproduce the A-B splitting within the  $sp_3s$  basis, a crystal field of 40 meV is added to the  $p_z$  local orbitals.<sup>21</sup>

### B. Time-dependent approach

Instead of diagonalizing the tight-binding Hamiltonian directly we employ the time-dependent approach which has been used previously to calculate electronic and excitonic properties of CdSe nanocrystals with zinc-blende structure.<sup>18</sup> In the following we will briefly describe the time-dependent tight-binding technique, indicate the differences compared with previous calculations, and show its advantage for calculation of  $g$ -factors.

The time-dependent method depends primarily on the spectral decomposition for an arbitrary initial state. Let  $\mathcal{E}_n$  be the complete set of eigenfunctions of the Hamiltonian. Any initial state  $j(0)$  can be expressed as the linear combination of the eigenfunctions

$$j(0) = \sum_n b_n \mathcal{E}_n \quad (1)$$

The wavefunction at a later time  $t$  is

$$j(t) = e^{iHt} j(0) = \sum_n b_n e^{iE_n t} \mathcal{E}_n \quad (2)$$

Projecting the wavefunction at time  $t$  onto the initial wavefunction and perform the Fourier transform on ends

$$\int_{-1}^1 dt e^{iEt} \langle j(0) | j(t) \rangle = \sum_n b_n^2 f(E - E_n) \quad (3)$$

Thus the resulting Fourier spectrum can give us the spectral weight of the initial state in the eigenfunction basis

and the eigenenergies of the eigenstates, provided that the eigenstates have non-zero overlap with the initial state. To get the total density of states one can sum over the spectral decompositions obtained using each wavefunction in a complete set as the initial state in term. The natural and convenient complete set to choose in the tight-binding framework is the direct product set of all local site orbitals, atomic-orbitals, and spin states. Then

$$\sum_n (E - E_n) = \sum_{i,j} \sum_{l=1}^Z \int_0^T dt e^{iE_n t} h_{i,j}(t) j_{i,j}(0) i \quad (4)$$

where  $j_{i,j}(0)i = | \text{site}; \text{orbital}; \text{spin} \rangle$ . To achieve  $\delta$ -function resolution one would need to have the infinite length record of the correlation function  $h_{i,j}(t)i$ . In practice only a finite length  $T$  of record is available, which gives rise to artificial sidebands around a broadened  $\delta$ -function approximation. The finite record length is taken into account by multiplying the right hand side of Eq. (4) with the normalized Hamming window function  $w(t)$ ,<sup>27</sup> where

$$w(t) = \begin{cases} 1 - \cos(\frac{2\pi t}{T}); & \text{if } 0 \leq t \leq T; \\ 0; & \text{if } t > T; \end{cases} \quad (5)$$

The window function will reduce the sidelobes of the broadened  $\delta$ -functions and generate a normalized peak height. The resulting spectrum is of the form

$$\sum_n W_n L(E - E_n) = \sum_{i,j} \sum_{l=1}^Z \int_0^T dt e^{iE_n t} w(t) h_{i,j}(t) j_{i,j}(0) i \quad (6)$$

where  $W_n$  represents the absolute spectral weight in eigenstate  $|E_n\rangle$  and the lineshape function  $L(E - E_n)$  is defined by

$$L(E - E_n) = \frac{e^{i(E - E_n)T}}{i(E - E_n)T} \frac{1}{2} \sum_{s=-1}^1 \frac{e^{i(E - E_n)T + 2s}}{i(E - E_n)T + 2s} \quad (7)$$

If the total wavefunction propagation time is  $T$ , the energy resolution is  $\Delta E = \pi/T$ . If the energy difference between the desired eigenenergy  $E_n$ , and adjacent eigenenergies is larger than  $\pi/T$ , the spectrum near energy  $E_n$  can be approximately represented by  $W_n L(E - E_n)$  with very high accuracy. Assuming this form, the value of the eigenvalue can be determined with accuracy much higher than  $\pi/T$ . To get the most accurate value possible it is desirable to perform the time integration of Eq. (6) by direct integration instead of using a discrete Fourier transform.

In order to use the spectral method one must be able to calculate the time propagator  $e^{-iHt}$  efficiently. In order to accomplish this we first break the time propagator into a series of short time propagators  $e^{-iHt} = (e^{-iH\Delta t})^N$  with  $t = N\Delta t$ . For the short time propagator we make

use of the Baker-Hausdorff formula<sup>9</sup> expansion to obtain the expansion

$$e^{-iH\Delta t} = e^{-i(H_1 + H_2)\Delta t} = e^{-iH_1\Delta t} e^{-iH_2\Delta t} + O(\Delta t^3) \quad (8)$$

To implement this decomposition we first break the tight-binding Hamiltonian into the on-site self-energy term  $s$ , the local spin-orbit term  $s$ , the local Zeeman term  $s$ , and the hopping term  $s$ . The on-site spin-orbit interaction is diagonalized and exponentiated analytically in the basis of the tight-binding orbitals, i.e. the  $6 \times 6$  matrix of the p-orbitals with spin. For the hopping term  $s$  we further use the checkerboard decomposition<sup>18,26</sup> to divide these to different independent directions. Note that in the zinc-blende structure there are only four fundamental directions while in the wurtzite structure there are seven fundamental directions. As a result of this decomposition each term contributing to the short time propagator can consequently be evaluated analytically<sup>18</sup> and the time evolution of the state can be calculated very efficiently.

The eigenfunction  $|E_n\rangle$  with eigenenergy  $E_n$  can be calculated from

$$|E_n\rangle = \sum_{i,j} \int_0^T dt e^{iE_n t} j_{i,j}(t) i \quad (9)$$

provided there is non-zero overlap between the initial wavefunction and the desired eigenfunction, i.e.  $\langle E_n | j_{i,j}(0) \rangle \neq 0$ . Typically when there is no magnetic field ( $B = 0$ ), the initial state is taken as a uniform superposition of local orbitals with specific angular momentum index. The resultant eigenfunctions are then used as the starting point to calculate the eigenfunctions and eigenenergies when the magnetic field is turned on.

If there are degenerate eigenstates, the right hand side of Eq. (9) will in general be some unknown linear combination of these eigenstates. However, if a set of exact or approximate quantum numbers which can be used to label the degenerate eigenstates are known in advance eigenfunctions corresponding to definite quantum numbers can be derived by judiciously choosing an initial state having the same quantum numbers. Typically the angular momentum index is used in this work for this purpose. This property will be used to generate Kramers' doublets in our calculations.

There are three important energy scales in this problem. The first energy scale is the energy difference between lowest conduction electron and higher energy conduction electrons and the difference between highest valence hole and lower energy hole states. This energy scale is typically at the order of 100 meV or larger. The second energy scale is the energy difference between nearly degenerate hole states that correspond approximately to the heavy hole and light hole states in the bulk limit. This energy scale is size dependent and is sensitive to the shape of the nanocrystals. In our calculation we find this energy scale to be 1-100 meV. The last important

energy scale is the magnetic field induced splitting for a Kramers' doublet from which the  $g$ -factors are extracted. Typically this energy scale ranges from couple of hundred eV to several eV.

The maximal total propagation time is about  $1280000 \text{ 1/eV}$ , resulting in an energy resolution of  $2.5 \text{ eV}$ . In our calculation this energy resolution is enough to single out the spectrum of band edge electron and hole states from other higher energy states. It is also sufficient to resolve the two nearly degenerate hole states. Once a high resolution eigenfunction is generated, by using window function Eq. (5-6) to suppress the contribution from adjacent eigenstates, the eigenenergies of band edge states can be determined with accuracy up to  $1 \text{ eV}$ .

### C. Calculation of the $g$ -factors

It is important to clarify the definition and the sign convention for the  $g$ -factors, especially when these  $g$ -factors are anisotropic. When there is no external magnetic field Kramers' theorem guarantees that each eigenstate is at least two fold degenerate. In bulk CdSe the heavy hole and light hole are degenerate at the  $\Gamma$  point. In a CdSe nanostructure it is expected that the quantum confinement will lift this degeneracy. In this work the  $g$ -factors will be defined with respect to the Kramers' doublet. For a Kramers' doublet the effective magnetic Hamiltonian has the form

$$H_e(B) = \sum_B B_B \sum_i^S G_i S_i; \quad (10)$$

where  $S$  is the effective spin operator, which is defined with respect to the two Kramers' states  $j_i$ , and  $G$  is the  $3 \times 3$   $g$ -factor tensor. In the Kramers' state basis, the effective spin operator  $S$  has the form

$$S_x = \frac{m}{2} \sigma_x; S_y = \frac{m}{2} \sigma_y; S_z = \frac{m}{2} \sigma_z; \quad (11)$$

where  $m$  is an integer chosen so that the real and effective spin are approximately equal. The  $G$  tensor can be diagonalized in the principal axes. Let  $\hat{e}_i, i = 1; 2; 3$  be the principal axes. Then an external magnetic field

$$B = B_1 \hat{e}_1 + B_2 \hat{e}_2 + B_3 \hat{e}_3 \quad (12)$$

will give rise to a Zeeman splitting

$$E(B) - (E(B) - E(0)) = \sum_B \sum_i^S g_i B_i; \quad (13)$$

We will denote the values  $g_i$  as principal  $g$ -factors. Individual  $g_i$  can be identified via varying external magnetic field along each of the principal directions and calculating the field dependent Zeeman splitting.

In our calculation for CdSe nanocrystal we find that the conduction electron is primarily  $s$ -like. In this case one can identify the effective spin operator with the real

spin operator and give the  $g$ -factors a definite sign. By choosing the initial wavefunction to have a well defined real spin index, the resultant eigenfunction will approximately have the corresponding effective spin index.

On the other hand, we find the hole to be primarily  $p$ -like. Furthermore, there is a strong mixing between heavy hole and light hole component which is sensitive to the size and the shape of the nanostructures. It is thus difficult to link the effective spin to the real spin, resulting in an ambiguity of the sign of the hole  $g$ -factors. In this situation it is more appropriate to express the Zeeman splitting by the quadratic form

$$E^2(B) - (E(B) - E(0))^2 = \sum_B \sum_i^S g_i^2 B_i^2; \quad (14)$$

in which the sign of principal  $g$ -factor is not well defined. Typically the sign convention of the  $g$ -factor in the atomic and bulk limit can then be used as a convention to assign an definite sign to the  $g$ -factors in the nanostructure. In both cases there usually exists a simple relation between the effective spin operator and real spin operator, which enables us to determine the corresponding sign of the  $g$ -factor in the nanostructure. However there is a dearth for experimental results of electron, hole, and exciton  $g$ -factor in bulk CdSe. Hence it is difficult in this case to use bulk experimental results as a guide to determine the sign of the  $g$ -factors.

In order to assign the sign to the hole  $g$ -factors for CdSe we therefore adopt the following scheme. The hole wavefunction will be calculated by propagating an initial state which has definite angular momentum index  $j = 3; j_z = 3; 2; 1; 2$ . The sign is then determined by whether the magnetic field induced energy shift is positive or negative. In the bulk limit this scheme will reproduce the heavy hole and light hole value correctly. In our calculation we find that the electron  $g$ -factor decreases as the size increases. This represents qualitatively the same trend as seen in effective mass type calculations<sup>2</sup> for various semiconductor nanostructures. On the other hand the calculated hole  $g$ -factor for CdSe shows oscillations, making correlation with the atomic and bulk limits more difficult.

### D. Gauge invariance

Since in this work the  $g$ -factors will be determined via the energy splitting of the electron and hole states under the external magnetic field, it is critical to cast the tight-binding model into a gauge invariant form. We use the Peierls-coupling tight-binding scheme to ensure the gauge invariance in our tight-binding model.<sup>28,29,30</sup> In this scheme an electromagnetic field specified by the scalar potential  $\phi(\mathbf{r}; t)$  and the vector potential  $\mathbf{A}(\mathbf{r}; t)$  will modify the on-site  $h_i; R_{ij}; R_{ji}$  and off-site  $h^0; R_{ij}^0; R_{ji}^0$  tight-binding parameters via

TABLE I: Size, diameters, and aspect ratio of the nanostructures.

| Number of atoms | 66    | 108   | 144   | 237   | 336   | 384   | 450   | 561   | 758   | 768   | 777   | 1501  |
|-----------------|-------|-------|-------|-------|-------|-------|-------|-------|-------|-------|-------|-------|
| $L_x L_y$ (Å)   | 13.38 | 13.38 | 16.92 | 21.85 | 21.85 | 25.39 | 26.76 | 22.85 | 34.55 | 27.42 | 20.44 | 43.01 |
| $L_z$ (Å)       | 11.38 | 18.38 | 18.38 | 14.88 | 21.88 | 24.38 | 21.88 | 35.88 | 35.88 | 39.38 | 49.88 | 42.88 |
| Aspect Ratio    | 0.85  | 1.37  | 1.09  | 0.68  | 1.00  | 0.99  | 0.82  | 1.64  | 1.04  | 1.44  | 2.44  | 0.99  |

$$h; R_i | H_j; R_i | \neq h; R_i | H_j; R_i | \quad (R_i; t); \quad (15)$$

and

$$h^0; R_i^0 | H_j; R_i | \neq h^0; R_i^0 | H_j; R_i | e^{i \frac{R_i^0}{R_i} \mathbf{R}(\mathbf{r}; t)} \quad (16)$$

where a straight line should be taken for the vector potential integral. In this calculation, the on-site intra-atomic dipole matrix elements  $\langle i | j \rangle$  and  $\langle i | i \rangle$  are set to zero. As pointed out by Foreman<sup>22</sup>, this choice ensures gauge invariance but cannot correctly describe intra-atomic transitions in the atomic limit. However, predictive calculation of atomic transitions is not contained within empirical tight-binding treatment. Previously, optical absorption spectra have been dealt with in tight-binding analysis by incorporating dipole matrix elements as extra fitting parameters. For CdSe nanocrystals, calculation of the bulk absorption spectrum has been found to be insensitive to the magnitude of the on-site dipole matrix elements<sup>19,20,21</sup>. This provides some empirical justification for setting these matrix elements to zero in order to achieve gauge invariance.

For gauge-invariant correction we thus only need to modify the hopping constant between nearest neighbors. Since there are only seven independent hopping directions in a wurtzite structure the gauge phase can be calculated and stored before performing the time propagation. A brief summary of the gauge phase in the wurtzite structure is given in the appendix A.

To estimate the contribution to the Zeeman splitting from the gauge phase, we have calculated the Zeeman splitting without gauge phase for some of the nanocrystals. We find that the gauge phase contributes 10-40%

of the Zeeman energy. Without the gauge phase the Zeeman splitting increases and becomes more isotropic.

### III. RESULTS

We investigate CdSe nanostructures having 66-1501 atoms. This roughly corresponds to the size range of 15-43 Å in the effective diameter. In our calculation we define the aspect ratio to be the ratio between the effective in-plane diameter ( $\sqrt{L_x L_y}$ ) and out-of-plane diameter ( $L_z$ ). The aspect ratio of these nanostructures ranges from 0.68 to 1.64. These can be divided into three different aspect ratio groups. The first group has aspect ratio well below one, ranging from 0.68 to 0.85. The second group has aspect ratio approximately equal to one, ranging from 0.99 to 1.09. The third group has aspect ratio well above one, ranging from 1.37 to 1.64. A nanostructure with aspect ratio 2.44 is also studied, in order to probe the trends of g-factors in the quantum rod limit. In Table I we summarize the in-plane diameter and out-of-plane diameter values of the nanostructures. If the aspect ratio of the nanostructures deviate from 1.0 by less than 10% then it is appropriate to use a single effective diameter ( $\sqrt{L_x L_y}$ ) to characterize the nanostructure. Note that the nanostructures used in the TRFR experiment have reported aspect ratios in the range of 1.17-1.34.<sup>2</sup> However a single effective diameter was nevertheless used to characterize the nanostructures. Furthermore, the TRFR sample has 5-15% size distribution and 0.2 aspect ratio variation. Hence, one must be cautious when making a quantitative comparison between the calculated and the experimental results.

To verify that the tight-binding model can reproduce the general features of conduction band, valence band, and identifiable band gap for nanostructures we have calculated the total density of states (TDOS) for smaller nanostructures (66-450 atoms). In Fig. 1 we plot the low resolution ( $\sim 50$  meV) TDOS for a 450 atom CdSe nanocrystal. It is evident from the figure that the conduction band edge (CBE), valence band edge (VBE), and band gap can be easily identified. It should be noted that the TDOS calculation is computationally expensive because one has to sum over a complete set of initial states. How-

ever only the states at the band edges are relevant to the optical orientation experiment. A prior knowledge of the TDOS is not necessary for calculation of the band edge eigenstates. A reasonable initial guess of the band edge eigenenergy is sufficient for calculation of high resolution band edge eigenenergies and eigenfunctions through an iterative procedure described below. For the smaller nanostructures where we have calculated the TDOS, we use the band edge energies identified from the TDOS data as initial values. For the larger nanostructures, we assign the initial value of band edge energies by extrapolating

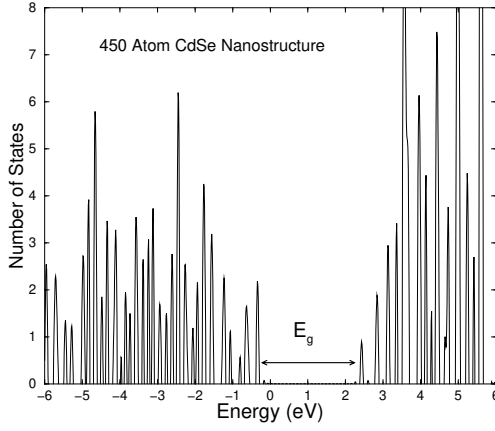


FIG. 1: Total density of states for a 450 atom CdSe nanocrystal.

the band edge energies of the smaller nanostructures.

To get the high resolution band edge eigenenergies and eigenstates we first estimate the eigenenergies as described above. A low resolution eigenstate is then generated using some judiciously chosen initial state. The initial state is set up to have non-zero overlap with the desired eigenfunction and to possess a well-defined value of some particular quantum number such as the  $z$ -component of the local total angular momentum  $j_j; j_z$ . This low resolution eigenstate is then put through the spectral weight analysis described in section IIB which results in a higher resolution eigenenergy. The higher resolution eigenenergy is then used together with the lower resolution eigenstate to generate a higher resolution eigenstate. This process is iterated until the desired accuracy is acquired and, in the case of the hole, until the near degeneracy between heavy hole like and light hole like doublets is lifted. Once the CBE and VBE eigenenergies are found, the band gap can be trivially calculated, from  $E_{\text{Gap}} = E_{\text{CBE}} - E_{\text{VBE}}$ . In Fig. 2 we plot the high resolution results for the size dependent CBE energy, VBE energy, and band gap. These results are all stable with respect to further iteration. Note that the VBE consists of two nearly degenerate Kramers' doublets. As the size of the nanostructure increases, these two doublets will converge respectively to the heavy and light hole doublets in bulk CdSe.

#### A. Electron $g$ -factor

Although the CdSe nanostructures we studied here have only approximate but not exact  $C_{3v}$  symmetry, we

expect nevertheless that the principal axes are still located approximately along the  $x$ ,  $y$ , and  $z$  directions. This is supported by the result of a perturbative time-independent tight-binding calculation of  $g$ -factors for these same nanocrystals<sup>14</sup> in which it was found that  $g_x \approx g_y \approx g_z$ . To accurately identify the Zeeman

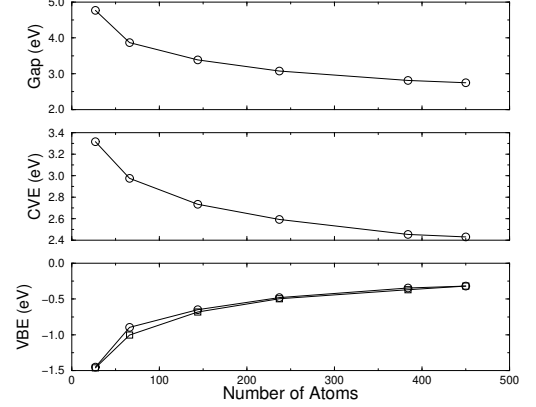


FIG. 2: (a) Band gap (b) CBE energy (c) VBE energy as a function of the number of atoms. Note that the VBE consists of two nearly degenerate levels in a CdSe nanocrystal, each corresponding to a perturbed Kramers' doublet, i.e. 4 states in total.

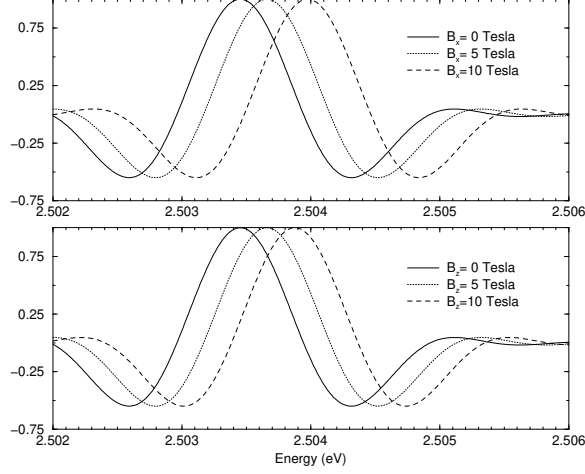
splitting it is necessary to generate the Kramers' doublet which will evolve into the Zeeman eigenstates when we turn on the external magnetic field. (This is essentially equivalent to solving the zeroth order degenerate perturbation problem.) The Kramers' doublet  $j^{\pm z}$  for a magnetic field pointing in the  $+z$ -direction can be generated via setting all local orbitals of the initial states to have spin equal to  $\frac{1}{2}$ . The Kramers' doublet for  $x$  and  $y$  directions are then calculated as  $j^{\pm x} = \frac{1}{\sqrt{2}}(j^{\pm z} \mp j^{\pm y})$  and  $j^{\pm y} = \frac{1}{\sqrt{2}}(j^{\pm z} \pm ij^{\pm x})$  respectively. The external magnetic field is limited to be less than 10 Tesla, which corresponds to the range of magnetic field in the typical experiments<sup>2,3</sup>. To make the connection to the CBE in the bulk material, which is  $s$ -like, we calculate the spectral weight of the  $j^{\pm z}$  state in the  $j_s = \frac{1}{2}$  local orbital of Cd and Se. In Table II we summarize the size dependence of these  $s$ -orbital spectral weights. We find that the CBE electron in the nanostructure is still primarily  $s$ -like, with spectral weights greater than 0.75 for all sizes. The  $s$ -orbital contribution increases monotonically as the size increases.

In Fig. 3 we plot the magnetic field dependent spectra for the  $j^{\pm x}$  state with magnetic field in the  $x$ -

direction and for the  $j^{\pm z}$  state with magnetic field in the  $z$ -direction, for a 336 atom CdSe nanocrystal. As-

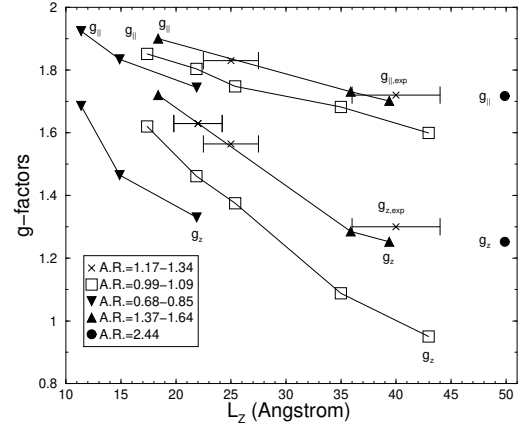
TABLE II: Spectral weight of  $j^+z$  in the  $j_z = \frac{1}{2}i$  local orbital of Cd and Se.

| Number of atoms      | 66   | 108  | 143  | 237  | 336  | 384  | 450  | 561  | 758  | 768  | 777  | 1501 |
|----------------------|------|------|------|------|------|------|------|------|------|------|------|------|
| $j_z = \frac{1}{2}i$ | 0.75 | 0.79 | 0.81 | 0.83 | 0.85 | 0.86 | 0.86 | 0.88 | 0.87 | 0.88 | 0.89 | 0.90 |

FIG. 3: Zeeman shift of the  $j^+x$  component of the Kramers' doublet in the CBE when (a) the external field  $B$  is in the  $+x$ -direction and (b) the  $+z$ -direction.

suming the spectral peaks have lineshapes of the form  $L(E - E_n(B))$ , the magnetic field dependent eigenenergy  $E_n(B)$  can then be determined with very high accuracy. The  $g$ -factor is then extracted by fitting  $E_n(B)$  as a function of  $B$ . In Fig. 4 we plot the resulting electron  $g$ -factors as a function of the length parameter  $L_z$ . The data are grouped according to the aspect ratio of the nanostructure. Group 1 (down triangles) has aspect ratio 0.68–0.85, group 2 (open squares) has aspect ratio 0.99–1.09, and group 3 (up triangles) has aspect ratio 1.37–1.64. One calculation for nanocrystal with aspect ratio 2.44 is also included (closed circle). The extracted  $g$ -factors from TRFR experiments<sup>2</sup> are also plotted for comparison (asterisks). Note that the size distribution of the sample in the TRFR experiments is about 5–15%, which is represented in the figure by the horizontal error bar. The aspect ratio of the sample in TRFR experiment in this size range is about 1.17–1.34, with a 0.2 variation.

From the calculations we find that  $g_x = g_y > g_z$  for all the nanostructures. As a result only two sets of data are shown in the figure and  $g_x$  is used to represent both  $g_x$  and  $g_y$ . The results show strong anisotropy between  $g_z$  and  $g_k$ . Both  $g$ -factors decrease monotonically as a function of the size of the nanostructure. The value of  $g_z$  decreases rapidly, while the value of  $g_k$  decreases more gradually. Fig. 4 shows that our results are in good agreement with the experimental values. It is evident from the figure that when there are two distinct  $g$ -factors observed for a given nanostructure, they should be identified with the in-plane ( $g_k$ ) and out-of-plane ( $g_z$ )  $g$ -factors of the electron. This assignment is very different from the

FIG. 4: CdSe nanocrystal electron  $g$ -factors as a function of the nanocrystal length parameter  $L_z$ .

original experimental suggestion that one of the  $g$ -factors should be identified with the isotropic electron  $g$ -factor while the other  $g$ -factor might be identified with an exciton  $g$ -factor.<sup>2</sup>

It is intriguing to look into the aspect ratio dependence of the  $g$ -factors in more detail. We observe from Fig. 4 that both  $g_k$  and  $g_z$  increase as the aspect ratio increases, provided that the aspect ratio is less than 1.64. We find that  $g_z$  is more sensitive to the aspect ratio and increases much more with this than  $g_k$ . The  $g$ -factors begin to saturate between aspect ratio 1.64 and 2.44. It is expected that if one continues to increase the aspect ratio then  $g_z$  should begin to decrease, since it eventually should approach the bulk value. On the other hand  $g_k$  should stay roughly constant after it saturates, provided that the in-plane cross-section is kept the same when one increases the aspect ratio. It should be emphasized that the aspect ratio is only a simple indicator for the shape of the nanostructure. Two nanostructures with similar number of atoms and aspect ratio values might still have very different shape or surface structure. From the observations above it is clear that we can identify a range of aspect ratios in which the effect of anisotropy of the wurtzite structure and that of the shape of the nanocrystal partially cancel each other so that the electron  $g$ -factors become more isotropic. In the cases studied here it appears that the cancellation is not complete. It also appears unlikely from these exact calculation of  $g$ -factors that the cancellation will become more complete for large-size nanocrystals since the difference between  $g_z$  and  $g_k$  increases for larger nanocrystals having aspect ratio approximately unity. As a result a true quasi-spherical regime as predicted by an analysis perturbative in spin<sup>12,14</sup> in which the electron  $g$ -factors be-

TABLE III: Spectral weight of  $h_1$  state in the local orbitals  $jj = \frac{3}{2}; j_z i$ : (See text.)

| Number of Atoms      | 66   | 108  | 144  | 237  | 336  | 384  | 450  | 561  | 758  | 768  | 777  | 1501 |
|----------------------|------|------|------|------|------|------|------|------|------|------|------|------|
| $j_z = +\frac{3}{2}$ | 0.47 | 0.03 | 0.27 | 0.82 | 0.06 | 0.30 | 0.81 | 0.06 | 0.87 | 0.37 | 0.51 | 0.88 |
| $j_z = +\frac{1}{2}$ | 0.12 | 0.78 | 0.24 | 0.02 | 0.78 | 0.21 | 0.03 | 0.79 | 0.02 | 0.11 | 0.34 | 0.03 |
| $j_z = -\frac{1}{2}$ | 0.29 | 0.00 | 0.37 | 0.04 | 0.04 | 0.39 | 0.06 | 0.05 | 0.04 | 0.18 | 0.02 | 0.04 |
| $j_z = -\frac{3}{2}$ | 0.01 | 0.03 | 0.02 | 0.00 | 0.04 | 0.02 | 0.02 | 0.02 | 0.00 | 0.25 | 0.00 | 0.00 |

TABLE IV : Spectral weight of  $h_2$  state in the local orbitals  $jj = \frac{3}{2}; j_z i$ : (See text.)

| Number of Atoms      | 66   | 108  | 144  | 237  | 336  | 384  | 450  | 561  | 758  | 768  | 777  | 1501 |
|----------------------|------|------|------|------|------|------|------|------|------|------|------|------|
| $j_z = +\frac{3}{2}$ | 0.02 | 0.46 | 0.04 | 0.46 | 0.64 | 0.40 | 0.36 | 0.53 | 0.37 | 0.37 | 0.35 | 0.04 |
| $j_z = +\frac{1}{2}$ | 0.06 | 0.20 | 0.03 | 0.03 | 0.10 | 0.13 | 0.13 | 0.33 | 0.17 | 0.11 | 0.10 | 0.83 |
| $j_z = -\frac{1}{2}$ | 0.08 | 0.13 | 0.37 | 0.35 | 0.09 | 0.17 | 0.41 | 0.02 | 0.37 | 0.19 | 0.43 | 0.02 |
| $j_z = -\frac{3}{2}$ | 0.68 | 0.07 | 0.43 | 0.00 | 0.08 | 0.22 | 0.01 | 0.01 | 0.01 | 0.23 | 0.06 | 0.06 |

come isotropic may never reached. Under certain growth conditions it is possible to synthesis CdSe nanostructures with zincblende structure.<sup>23</sup> It is expected that for zincblende CdSe nanocrystals, if the shape of the nanostructure has high symmetry then there will be only one isotropic g-factor.<sup>24</sup>

#### B. Hole g-factor

We have calculated the values of  $g_z$  for the two nearly degenerate valence band edge doublets, which will be denoted by  $h_1$  and  $h_2$ . We define  $h_1$  ( $h_2$ ) to be the highest (second highest) energy valence band state. To connect

the  $h_1$  and  $h_2$  states to the heavy and light hole states in the bulk material we calculate their spectral weight in local orbitals possessing definite angular momentum quantum number  $jj = \frac{3}{2}; j_z i$ . In Table-III (Table-IV) we summarize the spectral weight of the  $h_1$  ( $h_2$ ) states. We find that for the nanocrystals in the size range we are interested in, the mixing between the  $\frac{3}{2}$  and  $\frac{1}{2}$  components is very strong. The mixing also seems to be sensitive to the size of the nanocrystal, without any clear trend emerging. As a result it becomes improper to rigorously identify the  $h_1$  ( $h_2$ ) state with the heavy (light) hole states respectively, and we therefore set  $m = 1$  in Eq. (11) for all hole states.

In Fig.5 we plot the size dependent hole g-factors for those two hole doublets. The data has been regrouped into heavy-hole like and light-hole like states. For each size of the nanostructure we look at the spectral weight of  $h_1$  and  $h_2$  states and determine which is more heavy-hole-like. Similarly to the electron g-factors, the data for hole g-factors are also grouped by the nanocrystal aspect ratio. We observe that the two hole states have very different g-factors. Both holes show strong oscillations as a function of the size. It is important to clarify how these g-factors should approach the relevant bulk values when the size of the nanocrystal increases. In the bulk CdSe semiconductor, the valence band near the  $\Gamma$  point can be described by the Luttinger Hamiltonian.<sup>31</sup> The states  $j_z = \frac{3}{2}; \frac{3}{2} i$  and  $j_z = \frac{3}{2}; \frac{1}{2} i$  are associated with the heavy-hole and light-hole respectively. If the heavy-hole and light-hole are really degenerate, then Eq. (10) is actually not appropriate, since the nature of the  $J = \frac{3}{2}$  angular momentum has to be taken into account. If the heavy-hole and light-hole are not degenerate and the mixing between  $j_z = \frac{3}{2}; \frac{1}{2} i$  and  $j_z = \frac{3}{2}; \frac{3}{2} i$  components are small, then one can use Eq. (10) and set  $m = 3$  for the heavy-hole and  $m = 1$  for the light-hole in Eq. (11).

We speculate that the irregular mixing of local orbitals evident in Tables III and IV is the cause of the hole g-factor oscillation in nanocrystal size. From the table we observe that the  $h_1$  state becomes more and more heavy-hole like for nanocrystal with more than 450 atoms, provided that the aspect ratio is close to one. It is expected that as the size of the nanocrystal increases, the two hole states will eventually converge to the heavy-hole and light-hole respectively. One must then be careful when comparing the hole g-factors values calculated here with the bulk heavy-hole g-factor since the latter is usually defined with  $m = 3$  in Eq. (11).<sup>13</sup>

#### IV. SUMMARY AND DISCUSSION

We have calculated the g-factors of the conduction band edge electrons and valence band edge holes in CdSe nanostructures using the time-dependent tight-binding method. This allows an exact, non-perturbative analysis, with extremely high resolution of the Zeeman shifts. We observe that the electron g-factors are strongly anisotropic, with  $g_x = g_y > g_z$  for all nanocrystal



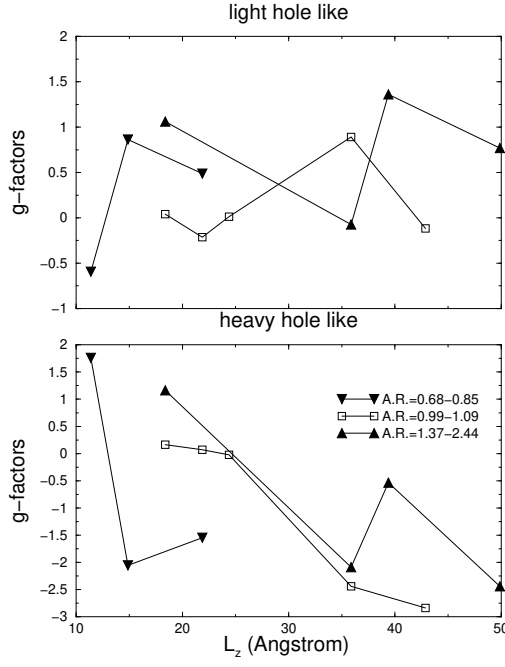


FIG. 5: CdSe nanocrystal hole g-factors as a function of the nanocrystal length parameter  $L_z$ .

sizes. The size dependence of the anisotropic electron g-factors agree quantitatively with the values extracted from TRFR experimental data. This leads to the conclusion that when there are two distinct g-factors in the TRFR experiments, they should be identified with the electron in-plane ( $g_k$ ) and out-of-plane ( $g_z$ ) g-factors respectively. This is very different from the original experimental suggestion that one of the g-factors is an isotropic electron g-factor while the other one is an exciton g-factor.<sup>2</sup> We have investigated the aspect ratio dependence of the electron g-factors. We find that in general the g-factors initially increase as a function of the aspect ratio, and that  $g_z$  increases more than  $g_k$ . The increase of g-factors saturates around aspect ratio 1.62-2.44. It is expected that  $g_z$  will then begin to decrease again until it reaches the bulk value while  $g_k$  will stay roughly the same, if the aspect ratio continue to increase. The aspect ratio dependence allows us to identify a regime where the anisotropy derived from the wurtzite structure and that derived from the shape of the nanocrystal cancel each other partially, resulting a more isotropic regime. However a full cancellation is never reached in our calculation, unlike the previous observation from a perturbative analysis.<sup>14</sup> It also appears unlikely that in larger nanocrystals the cancellation will become complete, since the difference between  $g_z$  and  $g_k$  for an unit aspect ratio nanocrystal increases as a function of the size.

We find that the valence band edge consists of two nearly degenerate Kramers' doublets, i.e. only a small perturbation from the bulk states. The hole g-factors for these states show oscillations as a function of the size. We speculate this is due to the strong size sensi-

tive heavy/light hole mixing of the two hole states.

One possible extension of the current calculation scheme is the evaluation of the exciton g-factors in these nanostructures. The g-factor of a uncorrelated electron-hole pair can be approximated by  $g_x = g_e - g_h$ . However the Coulomb interaction gives rise to excitonic effects and this simple picture then breaks down. The time-dependent tight-binding method has been successfully applied to calculate excitonic properties in CdSe nanocrystal<sup>18</sup> and it appears feasible to extend the current scheme to now calculate the corresponding exciton g-factors. Since the exciton fine structure splitting in CdSe nanocrystal is of the order 1-10 meV<sup>21</sup> the energy resolution obtained here ( $\sim 1$  V) is enough to resolve the exciton fine structure.

#### Acknowledgments

The authors acknowledge the financial support by the DARPA and ONR under Grant No. FDN 0014-01-1-0826 and by the ARO under Grant No. FDDAAD 19-01-1-0612. We thank NPACI for a generous allocation of supercomputer time at the San Diego Supercomputer Center. We also thank Dr. Seungwon Lee and Josh Schrier for fruitful discussions.

★

#### APPENDIX A

In the wurtzite structure there are 7 independent electron hopping directions. In this calculation these 7 hopping directions are denoted by  $\vec{a}_{\text{dir}}$ ,  $\text{dir} = 1 \dots 7$ , and are assigned to be the following vectors:

$$\begin{aligned} \vec{a}_1 &= \frac{a_0}{3} (0; 0; 3); \\ \vec{a}_2 &= \frac{a_0}{3} (2; \sqrt{2}; 0; 1); & \vec{a}_5 &= \frac{a_0}{3} (2; \sqrt{2}; 0; 1); \\ \vec{a}_3 &= \frac{a_0}{3} (2; \sqrt{2}; 0; 1); & \vec{a}_6 &= \frac{a_0}{3} (2; \sqrt{2}; 0; 1); \\ \vec{a}_4 &= \frac{a_0}{3} (2; \sqrt{2}; 0; 1); & \vec{a}_7 &= \frac{a_0}{3} (2; \sqrt{2}; 0; 1); \end{aligned} \quad (\text{A } 1)$$

Here  $a_0 = 2.625\text{\AA}$  is the lattice constant. This convention enables us to calculate the gauge-dependent quantities explicitly.

For a fixed external magnetic field  $\vec{B} = (B_x; B_y; B_z)$  we assign the vector potential to be  $\vec{A} = \frac{1}{2}\vec{B} \times \vec{r}$ . We define a magnetic-field-dependent gauge phase

$$(\vec{R}_a; \vec{a}_{\text{dir}}) = \frac{e}{\hbar} \int_{\vec{R}_a}^{\vec{R}_a + \vec{a}_{\text{dir}}} \vec{A} \cdot d\vec{l}; \quad (\text{A } 2)$$

where  $\vec{R}_a$  represents the position vector of an anion. The gauge phase for the cation can be easily calculated by taking the appropriate complex conjugation of the phase of the corresponding anion. With the line of integration to be a straight line, the integral can be calculated

analytically. Using this notation the gauge-dependent short-time propagation of the electron hopping in some particular direction becomes

$$e^{\hat{V}_{lm};dir dt} A_l j_{l-1}(\mathbf{R}_a) i + A_m j_m(\mathbf{R}_c) i \quad (A3)$$

$$= A_l \cos(V_{lm} dt) - i A_m \sin(V_{lm} dt) e^{+i(\mathbf{R}_a; \vec{d}_{dir})} j_{l-1}(\mathbf{R}_a) i$$

$$+ A_m \cos(V_{lm} dt) - i A_l \sin(V_{lm} dt) e^{-i(\mathbf{R}_a; \vec{d}_{dir})} j_m(\mathbf{R}_c) i;$$

where  $V_{lm}$  is the hopping constant in zero magnetic field.

- 
- <sup>1</sup> D. K. Young et al., *Semicond. Sci. Technol.* **17**, 275 (2002).
  - <sup>2</sup> J. A. Gupta, D. D. Awschalom, A. L. L. Efros, and A. V. Rodina, *Phys. Rev. B* **66**, 125307 (2002).
  - <sup>3</sup> J. A. Gupta, D. D. Awschalom, X. Peng, and A. P. Alivisatos, *Phys. Rev. B* **59**, R10421 (1999).
  - <sup>4</sup> A. V. Kadavanich, Ph.D. thesis, University of California, Berkeley, 1997.
  - <sup>5</sup> M. Kuno, M. Nimml, M. G. Bawendi, A. L. Efros, and M. Rosen, *J. Chem. Phys.* **108**, 4242 (1998).
  - <sup>6</sup> D. J. Hilton and C. L. Tang, *Phys. Rev. Lett.* **89**, 146601 (2002).
  - <sup>7</sup> T. Uenoyama and L. J. Sham, *Phys. Rev. Lett.* **64**, 3070 (1990).
  - <sup>8</sup> M. Paillard, et al. *Phys. Rev. Lett.* **86**, 1634 (2001).
  - <sup>9</sup> J. J. Sakurai, *Modern Quantum Mechanics* (Addison-Wesley, 1994).
  - <sup>10</sup> A. A. Kiselev, E. L. Ivchenko, and U. Rossler, *Phys. Rev. B* **58**, 16353, (1998).
  - <sup>11</sup> A. V. Rodina, A. L. L. Efros, M. Rosen, and B. K. Meyer, *Material Science and Engineering C* **19**, 435 (2002).
  - <sup>12</sup> A. V. Rodina, A. L. L. Efros, and A. Yu. Alekseev, *Phys. Rev. B* **67**, 155312 (2003).
  - <sup>13</sup> A. V. Nenashev, A. V. Dvurechenskii, and A. F. Zinovieva, *Phys. Rev. B* **67**, 205301 (2003).
  - <sup>14</sup> J. Schrier and K. B. W. Haley, *Phys. Rev. B* **67**, 235301 (2003).
  - <sup>15</sup> A. J. Stone, *Proc. Roy. Soc. A* **271**, 424 (1963).
  - <sup>16</sup> J. J. Shiang, A. V. Kadavanich, R. K. Grubbs, A. P. Alivisatos, *J. Phys. Chem.* **99**, 17417 (1995).
  - <sup>17</sup> P. E. Lippens and M. Lannoo, *Phys. Rev. B* **41**, 6079 (1990).
  - <sup>18</sup> N. A. Hill and K. B. W. Haley, *Chem. Phys.* **210**, 117 (1996).
  - <sup>19</sup> S. Pokrant and K. B. W. Haley, *Eur. Phys. J. D* **6**, 255 (1999); S. Pokrant, *Diplomarbeit*, Phillips-Universität Marburg, Marburg (1996).
  - <sup>20</sup> K. Leung and K. B. W. Haley, *Phys. Rev. B* **56**, 7455 (1997).
  - <sup>21</sup> K. Leung, S. Pokrant, and K. B. W. Haley, *Phys. Rev. B* **57**, 12291 (1998).
  - <sup>22</sup> B. A. Foreman, *Phys. Rev. B* **66**, 165212 (2002).
  - <sup>23</sup> L. M. Anna, E. C. Scher, and A. P. Alivisatos, *Jour. Cluster Science*, **13**, 521, (2002).
  - <sup>24</sup> S. Lee and K. B. W. Haley, unpublished.
  - <sup>25</sup> D. J. Chadi, *Phys. Rev. B* **16**, 790 (1977).
  - <sup>26</sup> M. Suzuki, *Prog. Theoret. Phys.* **56**, 1454 (1976).
  - <sup>27</sup> M. D. Feit, J. A. Fleck, Jr., and A. Steiger, *J. Comput. Phys.* **47**, 412 (1982).
  - <sup>28</sup> M. Graf and P. Vogl, *Phys. Rev. B* **51**, 4940 (1995).
  - <sup>29</sup> T. B. Boykin, R. C. Bowen, and G. Klimck, *Phys. Rev. B* **63**, 245314 (2001).
  - <sup>30</sup> T. B. Boykin and P. Vogl, *Phys. Rev. B* **65**, 035202 (2001).
  - <sup>31</sup> J. M. Luttinger, *Phys. Rev.* **102**, 1030 (1955).